Low-temperature properties of the $S = \frac{1}{2}$ spin system $Yb_3Ru_4Al_{12}$ with a distorted kagome lattice structure

S. Nakamura,[1,2,*] S. Toyoshima,[3] N. Kabeya,[2,3] K. Katoh,[4] T. Nojima,[1,2] and A. Ochiai[2,3,*]

[1]*Institute for Materials Research, Tohoku University, Sendai 980-8577, Japan*

[2]*Center for Low Temperature Science, Tohoku University, Sendai, Japan*

[3]*Department of Physics, Tohoku University, Sendai 980-8578, Japan*

[4]*Department of Applied Physics, National Defense Academy, Yokosuka 239-8686, Japan*

(Received 1 October 2014; revised manuscript received 24 May 2015; published 22 June 2015)

We have synthesized single crystals of ternary intermetallic $Yb_3Ru_4Al_{12}$ with a distorted kagome lattice structure, and investigated the low-temperature resistivity, specific heat, magnetization, and magnetic phase transitions. $Yb_3Ru_4Al_{12}$ is the first $4f$ system that has a $Gd_3Ru_4Al_{12}$-type crystal structure where antiferromagnetic interaction acts on the spin. The crystal electric field (CEF) ground state of this compound is determined as a well isolated twofold degenerate state that is subjected to a strong easy-plane-type magnetic anisotropy. In the present study, the spin system of $Yb_3Ru_4Al_{12}$ is regarded as an AFM XY model of $S = 1/2$. This compound undergoes successive magnetic phase transitions at 1.5 and 1.6 K, and the resistivity exhibits T^2 behavior below 1 K. The ratio of the coefficient of the T^2 term in the resistivity A, and that of the electronic specific heat coefficient γ_0, deviates from the Kadowaki-Woods (KW) law. The successive phase transitions and low-temperature properties of $Yb_3Ru_4Al_{12}$ where geometrical frustration and heavy fermion behavior occur are discussed.

DOI: 10.1103/PhysRevB.91.214426 PACS number(s): 71.27.+a, 75.30.Kz, 75.25.Dk

I. INTRODUCTION

There has been much effort on research into frustrated spin systems for more than a half century. Within the last two decades, the focus has also been on rare-earth compounds, such as magnetic pyrochlore oxides and heavy fermion compounds [1,2]. Among these, Yb compounds are attractive in that they exhibit various quantum spin states that reflect their crystal and electronic structures. For example, Yb_4As_3 is a mixed valence compound with a very low carrier density in which the mean valence of Yb ions is 2.25 [3,4]. This compound is known as a one-dimensional spin system. Yb_4As_3 undergoes a charge order with a decrease in temperature, which is associated with the cubic to trigonal structural phase transition at around 295 K. In association with this transition, magnetic Yb^{3+} ions form into four chains along the $\langle 111 \rangle$ direction, while other Yb ions assume a nonmagnetic divalent state [5]. The ground multiplet $J = 7/2$ of the Yb^{3+} ions splits into four doublets in the crystal electric field (CEF). In Yb_4As_3, the exchange interaction between the CEF doublet ground state is effectively expressed by the isotropic $S = 1/2$ antiferromagnetic (AFM) Heisenberg model [6]. Actually, the dispersion relation of neutron inelastic scattering peak of Yb_4As_3 is well explained by the $S = 1/2$ AFM Heisenberg chain [5,7]. For another example, the hexagonal low carrier compound $YbAl_3C_3$, Yb^{3+} ions form two-dimensional (2D) $S = 1/2$ triangular lattices in the ab plane [8,9]. A slight deformation of regular triangular lattice of Yb ions occurs in association with the structural transition from hexagonal to orthorhombic at 77 K [10,11]. The spin of the ground CEF state forms a spin-dimer state with the spin at a neighbor site [8–10,12]. The ground state of the dimer state is a nonmagnetic singlet and an triplet excited stays 15 K above. $YbAl_3C_3$ shows no magnetic ordering down to at least 40 mK in the absence of a magnetic field, but AFM ordering is induced by a magnetic field.

In metallic Yb compounds, Ruderman-Kittel-Kasuya-Yosida (RKKY) interaction acts on the magnetic ions via conduction electrons. This interaction often coexists with the Kondo effect through a wide range of Yb ion concentration. To date, a considerable number of Yb compounds have been identified as heavy fermion antiferromagnets (HFAFMs) [13]. Among them, several compounds are regarded as frustrated spin systems due to their geometrical structures. For example, YbPtIn and YbAgGe are HFAFMs that have a hexagonal ZrNiAl-type structure where Yb ions form a kagome-like lattice [14,15]. The enhanced electronic specific heat coefficient, γ_0, is estimated to be 430–740 mJ/(mol K^2) for YbPtIn and 200–370 mJ/(mol K^2) for YbAgGe [14,16–18]. The resistivity of YbPtIn exhibits T^2 behavior below 1 K at zero magnetic field, while YbAgGe shows Fermi liquid behavior at high fields [16,19]. Both compounds have complex magnetic phase diagrams at low temperatures [14,16,18,20]. Mössbauer absorption results indicate a partial disorder of Yb moments in YbPtIn, while it suggests ordered moments with a modulated amplitude in YbAgGe [16]. The multiple phase transitions and nonuniform amplitude of ordered moments are indicative of frustration in these spin systems.

The $RE_3Ru_4Al_{12}$ (RE: rare earth) ternary intermetallic compounds crystallize in a hexagonal structure of $Gd_3Ru_4Al_{12}$ type, where the RE-Al layers and nonmagnetic Ru-Al layers stack alternately along the c axis [see Figs. 1(a) and 1(b)] [21,22]. This crystal structure belongs to the $P6_3/mmc$ space group. In the RE-Al layer, RE ions construct a distorted kagome lattice composed of two different sized regular triangles and hexagons with unequal sides [see Fig. 1(c)]. The local symmetry on the RE site belongs to mmc. According to magnetization measurements, $La_3Ru_4Al_{12}$ is paramagnetic, while $Pr_3Ru_4Al_{12}$ and $Nd_3Ru_4Al_{12}$ are ferromagnetic [23]. $Ce_3Ru_4Al_{12}$ is considered to be a valence fluctuation system

*Corresponding authors: nakamura@imr.tohoku.ac.jp and aochiai@mail.clts.tohoku.ac.jp

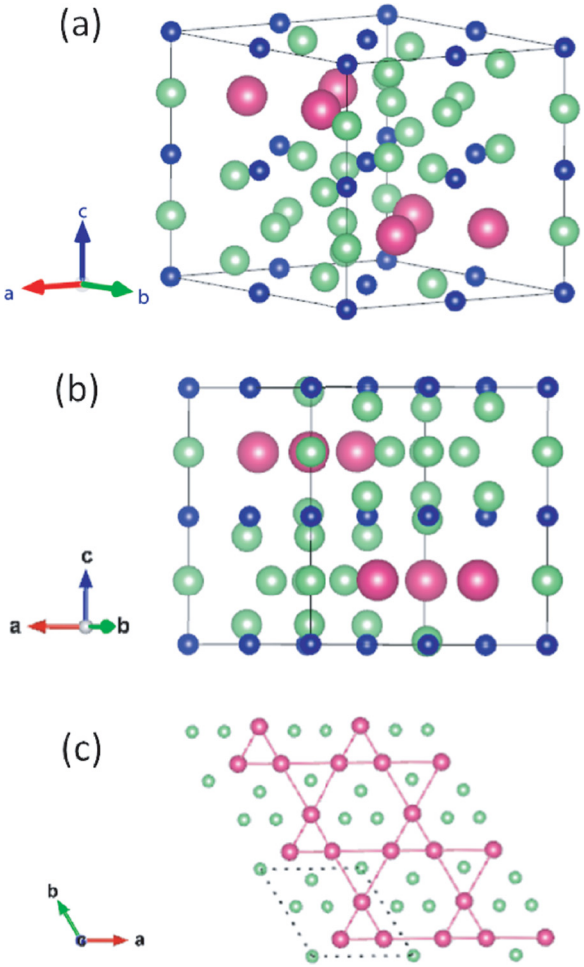

FIG. 1. (Color online) (a) Crystal structure of $Yb_3Ru_4Al_{12}$. The red (large), blue (small), and light green (middle) spheres denote Yb, Ru, and Al ions, respectively. (b) Crystal structure of $Yb_3Ru_4Al_{12}$ projected parallel to the *ab* plane. (c) Structure of a Yb-Al layer in $Yb_3Ru_4Al_{12}$ projected along the *c* axis over a wide range. The red (larger) and light green (smaller) spheres denote Yb and Al ions, respectively. The dotted rhombus displays the single unit cell. The bonds (red, solid lines) are drawn between nearest and second nearest Yb ions.

from the measured lattice constants [21]. $U_3Ru_4Al_{12}$ is an AFM compound with a Néel temperature T_N of 9.5 K [24]. The electronic specific heat coefficient γ_0 of $U_3Ru_4Al_{12}$ is enhanced to 200 mJ/(mol K^2), which implies a heavy fermion state. Although the range of the RKKY interaction is typically long, it is shortened by the Kondo effect due to the screening of magnetic moments and magnetic scattering of the conduction electrons. In such a situation, the short-range crystal structures, such as the triangular structure of Yb ions or layered structures of the lattice, may have a significant effect on the low-temperature properties and on the ground states of these spin systems.

In the present paper, we investigate the low-temperature properties and magnetic phase transitions of $Yb_3Ru_4Al_{12}$. We have succeeded to synthesize single crystals of $Yb_3Ru_4Al_{12}$ and polycrystals of the $Lu_3Ru_4Al_{12}$ reference system. In most metallic Yb compounds, the RKKY interaction is much weaker than the CEF. Therefore the magnetic anisotropy in Yb compounds at low temperatures is strongly dependent on the ground CEF state through the strong spin-orbit ($L - S$) coupling. When the magnetic anisotropy of the state is a very strong easy-plane type, the directions of the spins are limited in the plane. Based on this anisotropy by the CEF, the RKKY interaction acts on the spins as a perturbation, and as such, the spin system is regarded as an XY model. On the other hand, when the anisotropy is a strong easy-axis type, it is regarded as an Ising model. A brief report of this study has been presented at a conference [25].

II. SAMPLE PREPARATION AND EXPERIMENTAL

Ru was prereacted with Al using an arc furnace. The Ru-Al compound obtained was crushed and placed into tungsten crucibles with Yb pieces. The crucibles were sealed under high vacuum using an electron beam welding method. Single crystals of $Yb_3Ru_4Al_{12}$ were then grown by the Bridgman method and cubic single crystals with a size of a few millimeters were obtained. The crystal structure of this compound was determined using x-ray diffraction to be the same as that of $Gd_3Ru_4Al_{12}$ [21]. The *a*- and *c*-axis lattice constants obtained for $Yb_3Ru_4Al_{12}$ were 0.8732 and 0.9488 nm, respectively. For estimation of the phonon contribution to the specific heat, $Lu_3Ru_4Al_{12}$ polycrystals were prepared using the arc furnace. The crystal structure of this compound is the same as that of $Gd_3Ru_4Al_{12}$. The *a*- and *c*-axis lattice constants were determined as 0.8736 and 0.9476 nm, respectively.

The electrical resistivity was measured using the conventional dc four-terminal method. Measurements of the specific heat were performed using a thermal relaxation method with a commercial instrument (PPMS-9, Quantum Design Inc.). The magnetization was measured with a superconducting quantum interference device (SQUID) magnetometer (MPMS, Quantum Design Inc.) above 1.8 K and with a homemade Faraday balance magnetometer below 4.2 K down to 0.5 K. For measurements by the Faraday balance method, a superconducting magnet including coils for gradient fields (International Cryogenics Inc.) was used.

III. RESULTS

A. Transport properties

Let us begin by examining aspects of $Yb_3Ru_4Al_{12}$ as a Kondo system. Figure 2 shows the temperature dependence of resistivity for $Yb_3Ru_4Al_{12}$ at $H = 0$. Here, the current flows along the *a* and *c* axes. The resistivity has $\ln T$ characteristics in the range of $5 < T < 20$ K, regardless of the current direction, which indicates the Kondo effect. The Kondo temperature T_K is estimated to be approximately 10 K. At temperatures lower than 3 K, the resistivity decreases with the temperature. A break point in the resistivity for $I \parallel c$ at 1.6 K suggests a phase transition. An enlarged view of the resistivity for $I \parallel c$ at low temperatures is provided in the inset of Fig. 2 on a T^2 scale. The inset shows that the resistivity has T^2 behavior below 1 K, which implies that $Yb_3Ru_4Al_{12}$ is a heavy fermion compound. The solid line in the inset is a fit to the formula $\rho(T) = \rho_0 + AT^2$. It shows good agreement with the data over the range $0.33 < T^2 < 1$ K^2. The coefficient *A* obtained is 10.1 $\mu\Omega$ cm K^{-2}.

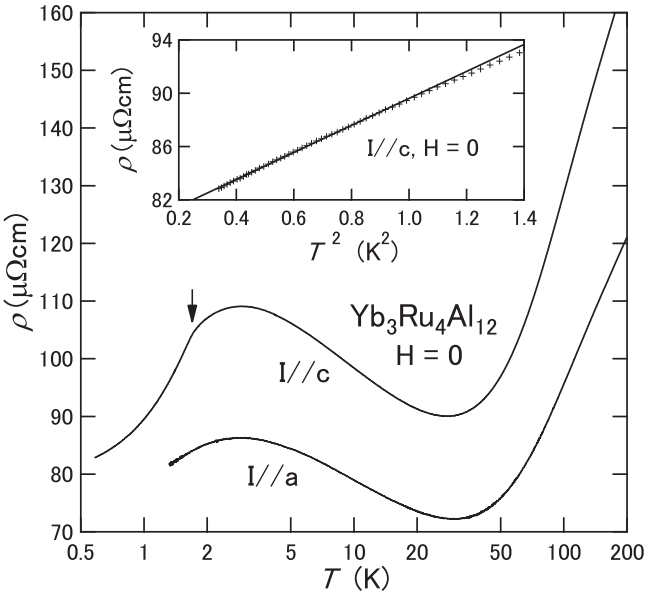

FIG. 2. Temperature dependence of the resistivity for $Yb_3Ru_4Al_{12}$ at $H = 0$ on a ln$T$ scale. The current is directed along the a and c axes. The arrow indicates the phase transition point. The inset shows an enlarged view of the resistivity for $I \parallel c$ on a T^2 scale. The solid line in the inset is a fit to the formula $\rho(T) = \rho_0 + AT^2$.

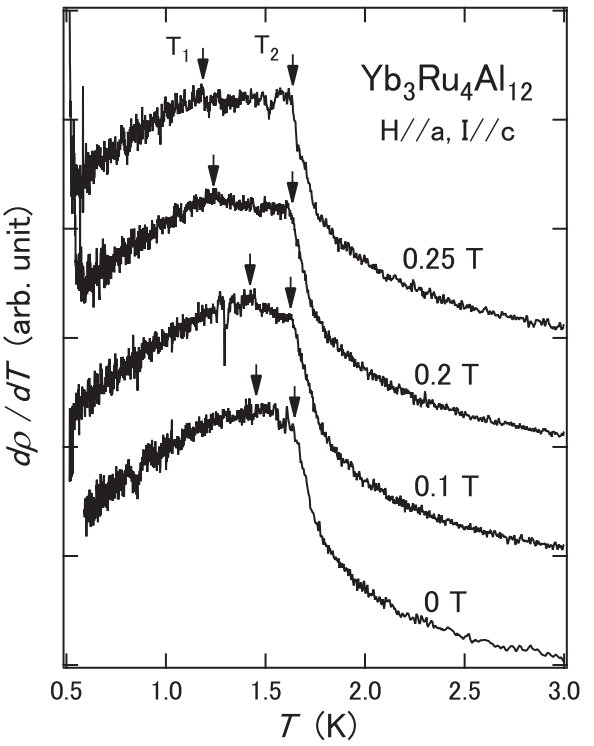

FIG. 3. Differential of the resistivity for $Yb_3Ru_4Al_{12}$ with respect to temperature at low fields. The fields are directed along the a axis and the current along the c axis. Arrows indicate the phase transition points. The origin points of the data are shifted for clarity.

The differentials of the resistivity with respect to temperature in the low field range are presented in Fig. 3. A clear anomaly suggests that a phase transition occurs at around 1.6 K for each field. This temperature is referred to as T_2. In addition to the anomalies at T_2, there are weak inflections at slightly lower temperatures, which is referred to as T_1. Figure 3 shows that T_1 shifts to the lower temperature side with increasing field, while T_2 remains almost independent of the field below 0.25 T. In the present paper, we refer to the phase below T_1 as phase I and to the intermediate-temperature phase as phase II. As discussed later, the successive phase transitions are supported by the specific heat and magnetization.

The field dependence for the resistivity of $Yb_3Ru_4Al_{12}$ with $H \parallel a$ and $I \parallel c$ is shown in Fig. 4. Negative magnetoresistivity is observed at each temperature, which is considered to be a suppression of the Kondo effect by the field. The inset shows an enlarged view of the data at 0.55 K. As shown in the main panel and the inset of Fig. 4, the resistivity has flat regions at fields lower than 0.25 T and below 1.3 K. In this field range, $Yb_3Ru_4Al_{12}$ is phase I. When the field is in the range of $0.25 < \mu_0 H < 1$ T, the resistivity decreases rapidly with an increase in the field. In this field range $Yb_3Ru_4Al_{12}$ is phase II. These two phases exhibit different response to the magnetic field.

The differential of the magnetoresistivity with respect to the field is presented in Fig. 5. The magnetoresistivity at 0.55 K reveals a small step at 0.25 T and a break point at 1.1 T. These transition fields are referred to as H_1 and H_2, respectively. H_1 corresponds to the phase I/phase II transition and H_2 to the phase II/para phase transition. H_1 and H_2 display a weak temperature dependence below 1.1 K.

B. Specific heat

The magnetic specific heat C_m of $Yb_3Ru_4Al_{12}$ for $H \parallel a$ is presented in Fig. 6. The specific heat of $Lu_3Ru_4Al_{12}$ $C_{\rm Lu}$ at zero field approximately follows the formula $C_{\rm Lu}(T) = 9.3 \times 10^{-3}T + 1.5 \times 10^{-4}T^3$ J/(K Lu mol) in the range $2.5 < T < 6$ K. The broken line in Fig. 6 denotes $C_{\rm Lu}(T)$ calculated by this formula. It is considerably small in comparison with the

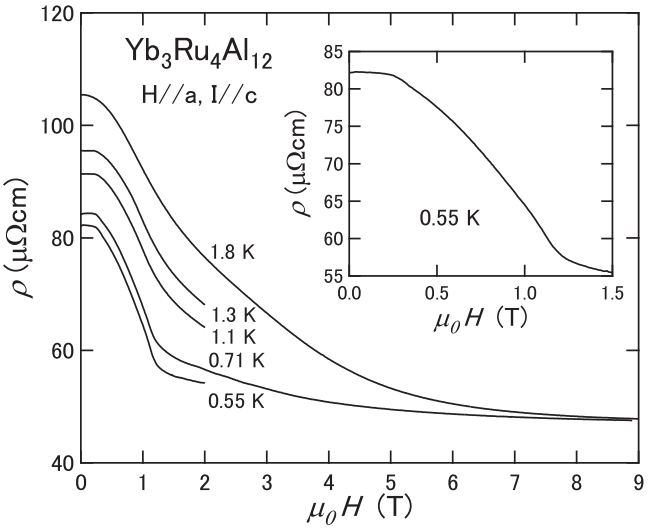

FIG. 4. Magnetoresistivity of $Yb_3Ru_4Al_{12}$, where the field and current are directed along the a and c axes, respectively. The inset shows the data for $T = 0.55$ K on an expanded scale.

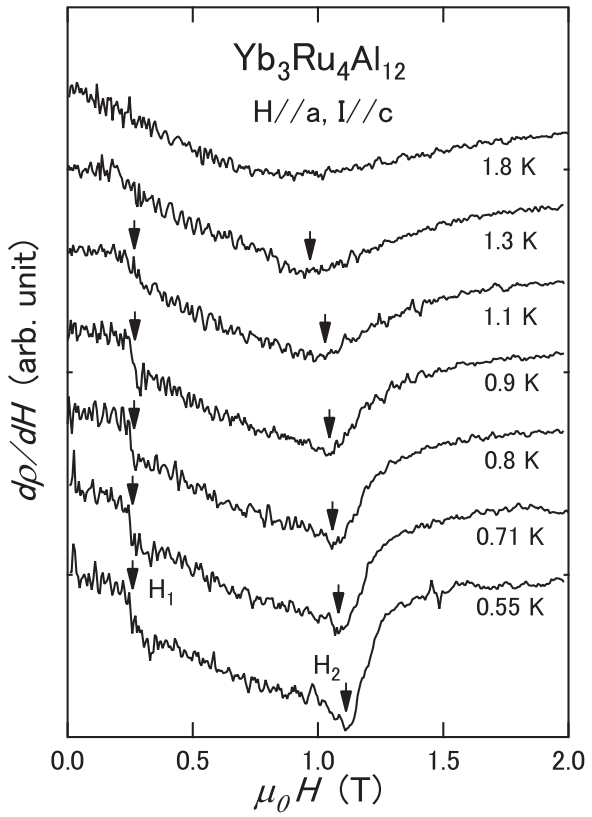

FIG. 5. Differential of the magnetoresistivity for $Yb_3Ru_4Al_{12}$ with respect to the field at several temperatures. The field and the current are directed along the a and c axes, respectively. Arrows indicate the phase transition points. The origin points of the data are shifted for clarity.

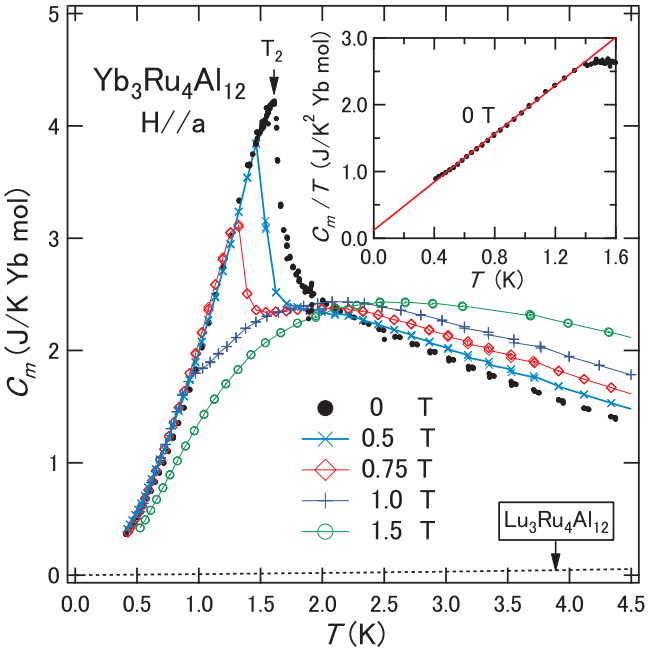

FIG. 6. (Color online) The magnetic specific heat of $Yb_3Ru_4Al_{12}$ per mole of Yb ions. The field is directed along the a axis. The inset shows the specific heat at zero field as a C_m/T-T plot. The solid line in the inset is a fit to the formula $C_m(T) = \gamma_0 T + \beta T^2$. This figure includes the specific heat of $Lu_3Ru_4Al_{12}$ per mole of Lu ions obtained by extrapolation of the data.

specific heat of $Yb_3Ru_4Al_{12}$ over the temperature range shown in this figure. For $H = 0$, the specific heat has a clear peak at around $T_2 = 1.6$ K and a long tail that extends to the higher temperature side. This peak is an indication of long-range ordering and it shifts to the lower temperature side with increasing field, but disappears at $\mu_0 H = 1.5$ T. The inset of Fig. 6 shows C_m/T for $H = 0$ as a function of T on an expanded scale. The solid line in the inset is a fit to the formula $C_m(T) = \gamma_0 T + \beta T^2$, which is in good agreement with the data below 1.4 K, i.e., in phase I. The T-linear term in the specific heat is interpreted as the electronic specific heat. The coefficient γ_0 obtained is 120 mJ/(K^2 Yb mol), which implies a heavy fermion state. The T^2 term can be explained in terms of the contribution of 2D AFM spin waves. The dispersion relation of the AFM spin waves is linear ($k \propto \omega$) when the wavelength is long. The contribution of 2D spin waves to the specific heat is, therefore, expected to be proportional to square of temperature [26]. Probably, the two dimensionality of the spin waves originates from the layered crystal structure of $Yb_3Ru_4Al_{12}$.

To elucidate the details of these phase transitions, we examine the specific heat in the low field range. The specific heat of $Yb_3Ru_4Al_{12}$ for $H \parallel a$ is displayed in Fig. 7 on an expanded temperature scale. The specific heat at $H = 0$ shows a kink at $T_1 = 1.45$ K in addition to the peak at T_2. This supports the double phase transitions separated even at zero field. The field dependence of T_1 is consistent with that shown in $d\rho/dT$ (Fig. 3). The anomalies in the specific heat at T_1 are considerably weak in comparison with those at T_2.

Figure 8 shows the temperature dependence of the magnetic entropy S_m, at $H = 0$. The entropy was calculated assuming that the phonon contribution to the specific heat of $Yb_3Ru_4Al_{12}$ is equal to that of $Lu_3Ru_4Al_{12}$. The entropy reaches $S_m = R\ln 2$ at around 20 K and has a clear shoulder, which indicates that the ground CEF state is a doublet and the first excited remains far above 20 K. The entropy gradually increases with the temperature and reaches $R\ln 8$, which is expected from the ground $J = 7/2$ multiplet of Yb^{3+} at around 300 K. For $Yb_3Ru_4Al_{12}$, the magnitude of CEF is much larger than that of the Kondo temperature. The inset in Fig. 8 shows S_m at low temperatures on an expanded scale, where S_m at $T_2 = 1.6$ K is approximately half of $R\ln 2$. Therefore, the lack of the entropy for $R\ln 2$ expected from the ground state is released above T_2. The long tail in the specific heat for $H = 0$ above 2 K shown in Fig. 6 corresponds this gradual release in entropy.

C. Magnetic susceptibility and magnetization

The magnetic susceptibility of $Yb_3Ru_4Al_{12}$ above 1.8 K is presented in Fig. 9. $Yb_3Ru_4Al_{12}$ is paramagnetic in this temperature range. The ratio of χ_a to χ_c at 1.8 K is 75. The magnetic anisotropy in $Yb_3Ru_4Al_{12}$ is very large and the ab plane is the easy plane. The inset in Fig. 9 shows that the magnetic susceptibility for $H \parallel c$ does not follow the Curie-Weiss law. χ_c^{-1} has a maximum at around 40 K and a minimum at around 150 K. These features are probably reflections of the CEF; however, the CEF states have not yet been determined.

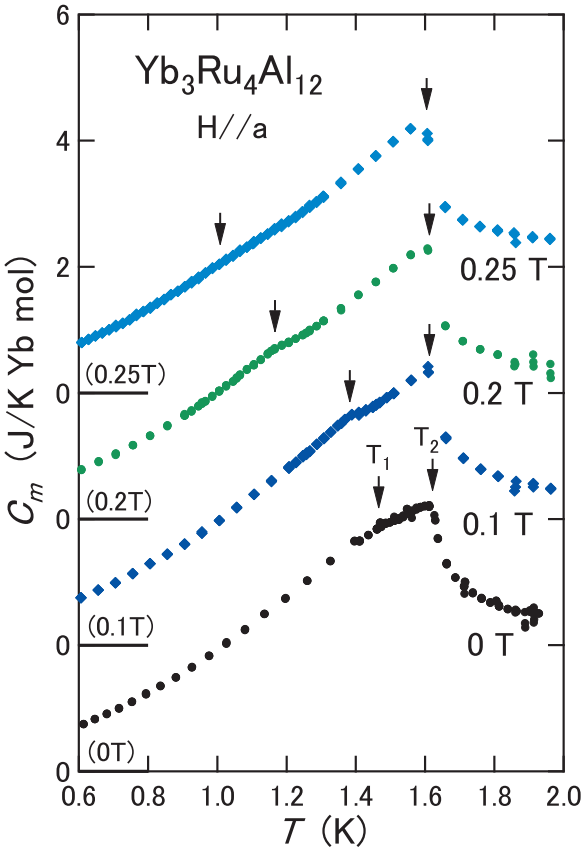

FIG. 7. (Color online) The magnetic specific heat of $Yb_3Ru_4Al_{12}$ per mole of Yb ions in the low-field range. The field is directed along the a axis. The origin point of the data at each field is shifted for clarity. The data for $H = 0$ are taken from Fig. 6.

Figure 10 shows the expanded temperature dependence of χ^{-1}, with χ^{-1} fitted in the temperature range of $2.2 < T < 10$ K, where the influence from excited CEF states is

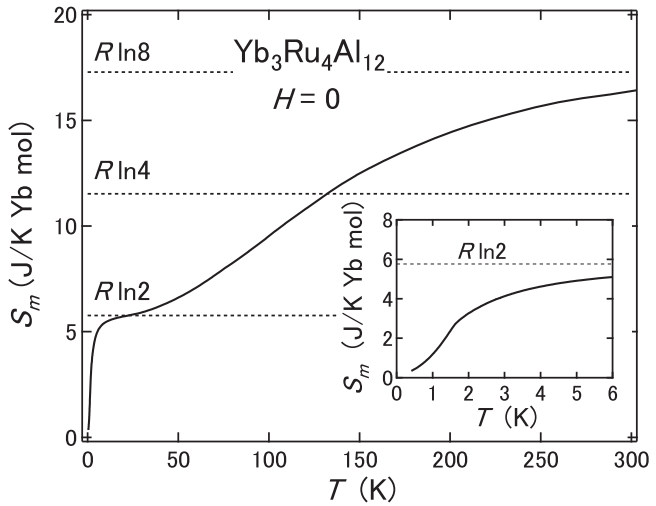

FIG. 8. The magnetic entropy of $Yb_3Ru_4Al_{12}$ at $H = 0$ calculated from the magnetic specific heat. The phonon contribution to the specific heat was assumed to be equal to that of $Lu_3Ru_4Al_{12}$. The inset shows the entropy in the low-temperature range on an expanded scale.

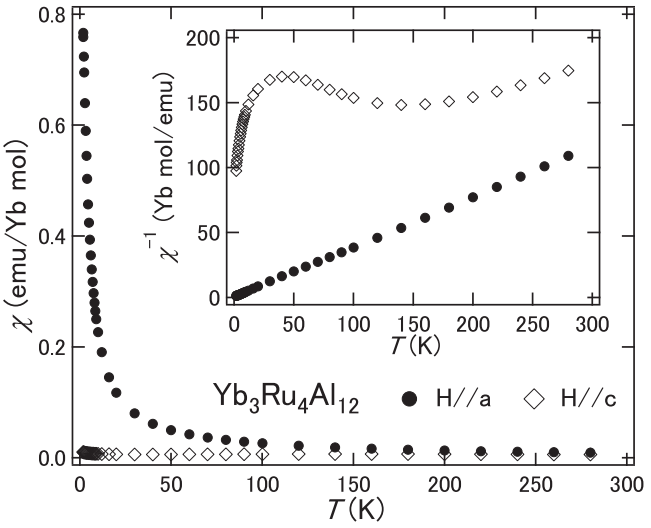

FIG. 9. Temperature dependence of the magnetic susceptibility for $Yb_3Ru_4Al_{12}$ measured using the MPMS magnetometer. The field is directed along the a (solid circles) and c axes (open diamonds). The amplitude of the applied field is 0.1 T. In this figure, the magnetic susceptibility is presented with respect to moles of Yb. The temperature dependence of the inverse magnetic susceptibility of $Yb_3Ru_4Al_{12}$ is presented in the inset.

negligible [27]. The solid circles in Fig. 10 are the data for $H \parallel a$ and the solid straight line represents a fit to the Curie-Weiss law, $\chi(T) = C/(T - \theta_p)$. The θ_p obtained is -1.15 K, which implies AFM interaction. The effective Bohr magnetron is determined as $p_{\rm eff} = 4.53$. The reduction in the magnitude of the effective magnetic moment due to the Kondo effect appears to be small in this temperature range. The open diamonds in Fig. 10 are the data for $H \parallel c$ and the solid curved

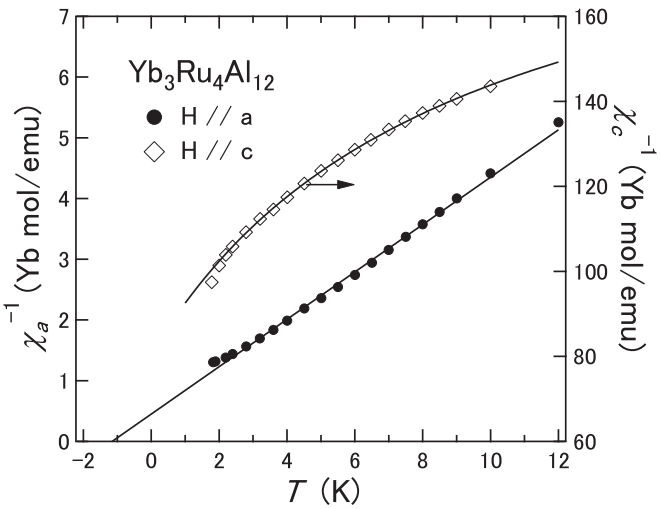

FIG. 10. Expanded temperature dependence of the inverse magnetic susceptibility for $H \parallel a$ (closed circles) and $H \parallel c$ (open diamonds). In this figure, the magnetic susceptibility is presented with respect to moles of Yb. The solid straight line is a fit to the Curie-Weiss law in the range $2.2 < T < 10$ K. The solid curved line is a fit to the formula $\chi = \chi_0 + C/(T - \theta_p)$ in the range $2.2 < T < 10$ K. Here, χ_0 is the Van Vleck term, which is assumed to be constant.

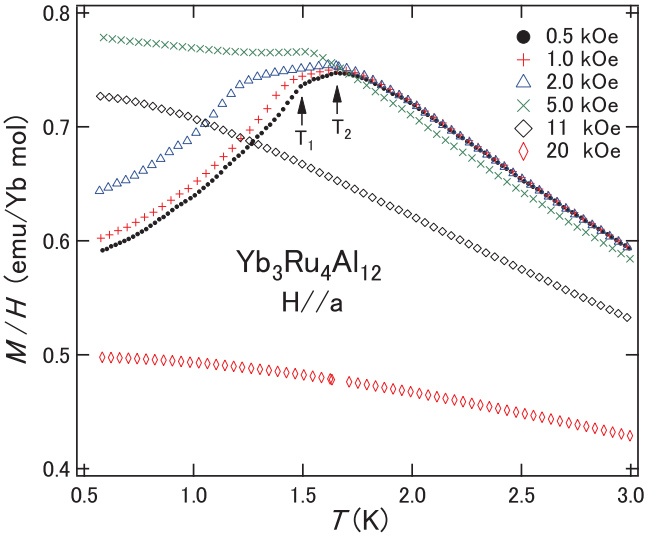

FIG. 11. (Color online) Temperature dependence of the magnetic susceptibility M/H, for $Yb_3Ru_4Al_{12}$ obtained at various fields directed along the a axis. The magnetic susceptibility is presented with respect to moles of Yb. The magnetization is measured using the Faraday balance magnetometer. Arrows indicate the transition temperatures at $H = 0$.

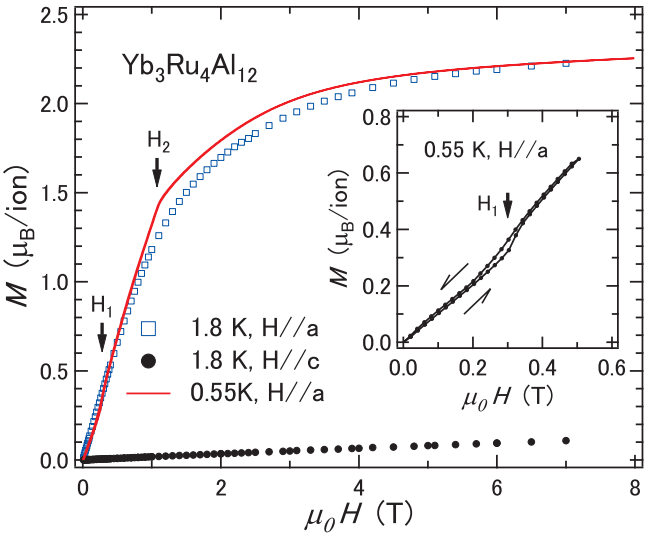

FIG. 12. (Color online) Field dependence of the magnetization for $Yb_3Ru_4Al_{12}$ represented by μ_B per Yb ion. Fields are directed along the a and c axes. Arrows indicate the transition fields at $T = 0.55$ K. The inset shows the magnetization hysteresis for $H \parallel a$ at 0.55 K.

line is a fit by the formula $\chi(T) = \chi_0 + C/(T - \theta_p)$. Here, we assumed the Van Vleck term χ_0 is constant at low temperatures. The parameters obtained are $\chi_0 = 5.0 \times 10^{-3}$ emu/mole, $\theta_p = -3.59$ K and $p_{\rm eff} = 0.46$. Probably, these values contain some error because the measurements of magnetic susceptibility for the hard axis are sensitive to the direction of the field when the anisotropy is very large. However, the direction of the magnetic moment in $Yb_3Ru_4Al_{12}$ is almost limited to the ab plane at low temperatures.

The magnetic susceptibility was measured at lower temperatures to clarify the properties of the ordered phases. Figure 11 shows the magnetic susceptibility M/H, for $Yb_3Ru_4Al_{12}$ obtained with various fields directed along the a axis. M/H for $H = 0.5$ kOe increases in the paramagnetic phase with a decrease in the temperature, and inflection points are observed at T_2 and T_1. Although the anomaly in the specific heat at T_1 is very small, an apparent inflection point in M/H is evident at this temperature. M/H only has a weak temperature dependence in the intermediate phase II, as shown in Fig. 11. In contrast, M/H has an apparent temperature dependence in phase I. Under the $H = 5.0$ kOe field, only one indication of a phase transition is observed. However, when the field becomes higher than 11 kOe, there is no indication of a phase transition.

Figure 12 shows the field dependence of the magnetization for $Yb_3Ru_4Al_{12}$. The magnetization at 1.8 K shows large magnetic anisotropy. The magnetization for $H \parallel c$ at 1.8 K is only 4.9% of that for $H \parallel a$ at 1.8 K, even at 7 T. The magnetization at 0.55 K has two anomalies at H_1 and at H_2. The magnetization hysteresis for $H \parallel a$ at 0.55 K is shown in the inset of Fig. 12, where a small hysteresis loop is observed at H_1. As shown in Fig. 12, saturated magnetization for $H \parallel a$ m_s at 0.55 K is estimated to be 2.3 μ_B. The magnetic entropy mentioned before indicates that the ground doublet state is well isolated from the first excited state. Therefore $p_{\rm eff}$ for the easy plane is given by using m_s as $p_{\rm eff}\mu_B = \sqrt{3}m_s$. Substituting 2.3 μ_B for m_s, we get $p_{\rm eff} = 4.0$. This is in good agreement with the value 4.53 obtained from the susceptibility mentioned before.

D. Magnetic phase diagram

The magnetic phase diagram for $Yb_3Ru_4Al_{12}$ with $H \parallel a$ was determined from a summary of the measurement results and is shown in Fig. 13. The field is directed along the a-axis. $Yb_3Ru_4Al_{12}$ undergoes two successive phase transitions at $H = 0$. Phase I occupies the low-T, low-H region, and is broken by weak fields. Phase II spreads to the intermediate field region; and is broken by fields higher than 1.1 T. A

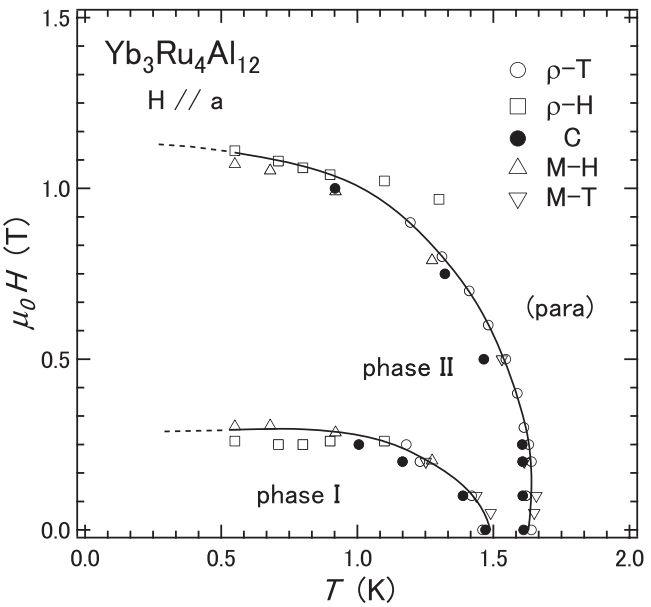

FIG. 13. Magnetic phase diagram for $Yb_3Ru_4Al_{12}$ in the H-T plane. The field is directed along the easy axis (a axis).

weak magnetization hysteresis is observed at H_1; therefore, the phase I/phase II transition is a weak first-order transition at finite fields.

IV. DISCUSSION

First, let us examine the characteristics of the $Yb_3Ru_4Al_{12}$ spin system. The magnetic anisotropy of $Yb_3Ru_4Al_{12}$ is the strong easy plane type. The magnetic entropy indicates that the ground CEF state is twofold degenerate and that the first excited state stays sufficiently higher than 20 K. Figure 13 shows that the ordered phases of $Yb_3Ru_4Al_{12}$ disappear under high fields. The Weiss temperatures θ_p, obtained from the magnetic susceptibility has a minus sign, which indicates that the AFM RKKY interaction acts on the spins. The magnitude of this interaction is estimated to be in the order of 1 K from the magnetic susceptibility, which is much smaller than the splitting between the ground CEF state and the first excited state. As such, the spin system of $Yb_3Ru_4Al_{12}$ is regarded as an AFM $S = 1/2$ XY-spin system at low temperatures. Very recently, Ge *et al.* reported low-temperature properties of polycrystalline $RE_3Ru_4Al_{12}$ (RE=La–Nd) [28]. Regardless of the difference in rare earth ions, some kinds of anomalies were observed in the magnetic susceptibility, resistivity or specific heat in the vicinity of 6 K. Ge *et al.* attributed these anomalies to the itinerant magnetism of Ru ions, which is independent of rare earth ions basically. However, in the cases of $RE_3Ru_4Al_{12}$ (RE=Yb, Lu), we could not find any indication of magnetic transitions at around 6 K. The present study is negative to the magnetism arising from Ru ions in these heavy rare earth compounds.

The low-temperature specific heat strongly suggests a 2D spin excitation in phase I, which indicates an anisotropic intersite interaction in $Yb_3Ru_4Al_{12}$. One possible explanation for the anisotropy in this interaction is the layered structure of this compound. The nonmagnetic layer is located between magnetic layers, therefore, the distance between the nearest Yb ions in different layers is long. Shortening of the range of the RKKY interaction by the Kondo effect would thus also contribute to a reduction in the interlayer interaction. Another possibility is the anisotropy of the band structure in $Yb_3Ru_4Al_{12}$. However, it can be concluded that the laminated crystal structure results in the two dimensionality of the $Yb_3Ru_4Al_{12}$ spin system.

Ever since the finding of the Kosteritz-Thouless (KT) transition that arises from degrees of rotational freedom, topological order in 2D XY-spin systems has attracted much attention [29]. When an isotropic frustration is introduced into a 2D XY-spin system on a square lattice, a long range order is expected to occur from the discrete degrees of freedom (Ising type) in addition to the KT transition [30–33]. A Monte Carlo simulation of the 2D AFM XY-spin system on a triangular lattice suggests two phase transitions of long range chiral order at T_c and quasi long range KT order at T_{KT} [34]. According to this simulation, T_{KT} is expected to be slightly lower than T_c, and a sharp peak in the specific heat and a weak break point in the susceptibility are predicted at T_c. A considerable number of theoretical studies on the AFM triangular lattice support the existence of a chiral ordered phase [35–38]. A recent simulation on a large size AFM triangular lattice predicted that a "spin order" occurs on the basis of chiral order at T_s ($\sim 0.9T_c$), which belongs to a different universality class of the KT phase [38]. A simulation on the 2D AFM XY model for a "regular" kagome lattice suggests the appearance of both chiral and KT phases [39].

In the present study, we have observed two successive phase transitions of $Yb_3Ru_4Al_{12}$. These transitions show some resemblance to the predicted chiral-KT or chiral-spin transitions. The points of resemblance are as follows: (1) two phase transitions occur with close temperatures at zero field. (2) The transition at higher temperature is accompanied by a clear specific heat peak, which indicates long range order. (3) The magnetic susceptibility of $Yb_3Ru_4Al_{12}$ shows a break point with a low folding angle at T_2. (4) The anomaly in the specific heat at lower temperature is very small, which suggests quasi-long-range order. There is a possibility that the phase transitions of $Yb_3Ru_4Al_{12}$ are topological. Thus microscopic measurements are required to confirm the magnetic phase characteristics of $Yb_3Ru_4Al_{12}$.

Next, we examine the heavy fermion aspects of $Yb_3Ru_4Al_{12}$. The temperature dependence of the specific heat in phase I is well explained by the contribution from heavy fermions and 2D AFM spin waves. In this phase, heavy-fermion-like behavior is evident both in the resistivity and specific heat. The ratio A/γ_0^2 is $7.0 \times 10^{-4}\,\mu\Omega$ cm(K mol/mJ)^2, which is approximately 70 times larger than that expected from the KW law [40,41]. A and γ_0 for $Yb_3Ru_4Al_{12}$ are presented in Fig. 14. The solid line in this figure indicates the relation between A and γ_0 expected from the KW law. For comparison, A and γ_0 of other typical heavy fermion compounds with twofold degeneracy ($N = 2$) are also presented in Fig. 14 [42–45]. CeB_6 and $CeAl_3$ with AFM ordering lie near the line with

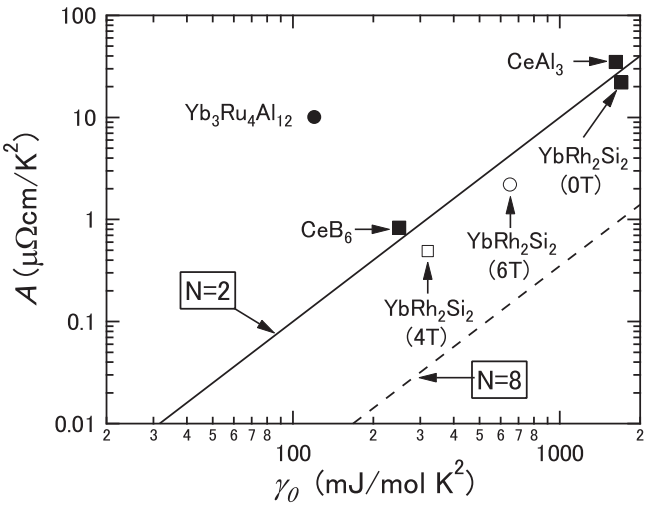

FIG. 14. The coefficient A vs γ_0 for heavy fermion compounds with twofold degeneracy ($N = 2$). The solid and broken lines indicate the KW relation $A/\gamma_0^2 = 1 \times 10^{-5}/[(1/2)N(N-1)]$ $\mu\Omega$ cm(K mol/mJ)^2 for $N = 2$ and 8, respectively. Data for $Yb_3Ru_4Al_{12}$ in phase I is thaken from the present results. Data for CeB_6 in the AFM phase is taken from Refs. [42] and [43]. Data for $CeAl_3$ in the AFM phase and $YbRh_2Si_2$ (closed square) in the AFM phase is taken from Refs. [44] and [45], respectively. This figure includes the data for $YbRh_2Si_2$ in the paramagnetic phase induced by the fields $H \parallel c$ (open circle) and $H \perp c$ (open square) taken from Ref. [45].

$N = 2$. $YbRh_2Si_2$ is a well known heavy fermion compound that exhibits magnetic-field-induced quantum critical phenomena [45]. This compound is AFM below 70 mK at 0 T, and transforms to a Fermi liquid without ordering at around 0.7 T. $YbRh_2Si_2$ is placed near the line with $N = 2$ regardless of the difference in phases, as shown in Fig. 14. This compound maintains the KW relation, even in the vicinity of the quantum critical point. In contrast, $Yb_3Ru_4Al_{12}$ apparently deviates from the line. Figure 14 contains a broken line that indicates the KW relation with $N = 8$. When T_K is much larger than CEF, the heavy fermions of Yb-compounds ($J = 7/2$) are situated around this line [41]. However, T_K for $Yb_3Ru_4Al_{12}$ is much smaller than the CEF. The orbital degeneracy shifts the line to the lower side, whereas the deviation of $Yb_3Ru_4Al_{12}$ is directed to the opposite side. The self-consistent renormalization theory that stands on the itinerant electron concept predicts that the instability in AFM leads to a deviation from the KW law [46]. According to this theory, the AFM instability increases A, whereas it does not influence γ_0. We suppose that the deviation from the KW law in $Yb_3Ru_4Al_{12}$ is related to the instability that arises from geometrical frustration.

V. CONCLUSION

We have successfully synthesized single crystals of $Yb_3Ru_4Al_{12}$ with a distorted kagome lattice structure and investigated their low-temperature properties. We have determined that $Yb_3Ru_4Al_{12}$ is the first compound with $Gd_3Ru_4Al_{12}$-type crystal structure where AFM interactions act on the spins. Strong easy-plane type magnetic anisotropy is observed in $Yb_3Ru_4Al_{12}$, where the directions of spin are almost limited in the ab plane. The specific heat implies that 2D spin waves are excited in phase I. The present results strongly suggest that the spin system of $Yb_3Ru_4Al_{12}$ is an example of the 2D AFM XY model. There is a possibility that the phase transitions of $Yb_3Ru_4Al_{12}$ are topological. However, the possibility that spontaneous magnetic moments are generated in these phases due to the incomplete two dimensionality is not excluded at the present time. Microscopic measurements are thus required for confirmation. $Yb_3Ru_4Al_{12}$ has exhibited heavy fermion behavior, both in the resistivity and specific heat; however, an apparent deviation from the KW law is observed, which may be related to the AFM instability arising from geometrical frustration.

ACKNOWLEDGMENTS

The authors thank S. Tanno, K. Hosokura, A. Ogata, M. Kikuchi, H. Moriyama, and N. Fukiage for their help with conducting the low-temperature experiments.

[1] For review, J. S. Gardner, M. J. P. Gingras, and J. E. Greedan, Rev. Mod. Phys. **82**, 53 (2010).
[2] For example, A. Dönni, G. Ehlers, H. Maletta, P. Fischer, H. Kitazawa, and M. Zolliker, J. Phys: Cond. Mat. **8**, 11213 (1996).
[3] A. Ochiai, K. Takeuchi, N. Niitsuma, T. Suzuki, and T. Kasuya, J. Mag. Mag. Mat. **63**, 618 (1987).
[4] A. Ochiai, T. Suzuki, and T. Kasuya, J. Phys. Soc. Jpn. **59**, 4129 (1990).
[5] M. Kohgi, K. Iwasa, J.-M. Mignot, A. Ochiai, and T. Suzuki, Phys. Rev. B **56**, R11388 (1997).
[6] H. Shiba, K. Ueda, and O. Sakai, J. Phys. Soc. Jpn. **69**, 1493 (2000).
[7] M. Kohgi, K. Iwasa, J.-M. Mignot, B. Fåk, P. Gegenwart, M. Lang, A. Ochiai, H. Aoki, and T. Suzuki, Phys. Rev. Lett. **86**, 2439 (2001).
[8] A. Ochiai, T. Inukai, T. Matsumura, A. Oyamada, and K. Katoh, J. Phys. Soc. Jpn. B **76**, 123703 (2007).
[9] K. Hara, S. Matsuda, E. Matsuoka, K. Tanigaki, A. Ochiai, S. Nakamura, T. Nojima, and K. Katoh, Phys. Rev. B **85**, 144416 (2012).
[10] S. K. Dhar, P. Manfrinetti, M. L. Fornasini, and P. Bonville, Eur. Phys. J. B **63**, 187 (2008).
[11] T. Matsumura, T. Inami, M. Kosaka, Y. Kato, T. Inukai, A. Ochiai H. Nakao, Y. Murakami, S. Katano, and H. S. Suzuki, J. Phys. Soc. Jpn. B **77**, 103601 (2008).
[12] Y. Kato, M. Kosaka, H. Nowatari, Y. Saiga, A. Yamada, T. Kobiyama, S. Katano, K. Ohoyama, H. S. Suzuki, N. Aso, and K. Iwasa, J. Phys. Soc. Jpn. **77**, 053701 (2008).
[13] For example, Z. Fisk and M. B. Maple, J. Alloy Comp. **183**, 303 (1992).
[14] O. Trovarelli, C. Geibel, R. Cardoso, S. Mederle, R. Borth, B. Buschinger, F. M. Grosche, Y. Grin, G. Sparn, and F. Steglich, Phys. Rev. B **61**, 9467 (2000).
[15] K. Katoh, Y. Mano, K. Nakano, G. Terui, Y. Niide, and A. Ochiai, J. Mag. Mag. Mat. **268**, 212 (2004).
[16] D. Kaczorowski, B. Andraka, R. Pietri, T. Cichorek, and V. I. Zaremba, Phys. Rev. B **61**, 15255 (2000).
[17] P. Bonville, M. Rams, K. Królas, J.-P. Sanchez, P. C. Canfield, O. Trovarelli, and C. Geibel, Eur. Phys. J. B **55**, 77 (2007)
[18] K. Umeo, K. Yamane, Y. Muro, K. Katoh, Y. Niide, A. Ochiai, T. Morie, T. Sakakibara, and T. Takabatake, J. Phys. Soc. Jpn. **73**, 537 (2004).
[19] S. L. Bud'ko, E. Morosan, and P. C. Canfield, Phys. Rev. B **69**, 014415 (2004).
[20] S. Yoshii, K. Kindo, K. Katoh, Y. Niide, and A. Ochiai, J. Mag. Mag. Mat. **272-276**, e99 (2004).
[21] J. Niermann and W. Jeitschko, Z. Anorg. Allg. Chem. **628**, 2549 (2002).
[22] Drawing of the crystal structure was produced using VESTA, K. Momma and F. Izumi, J. Appl. Cryst. **44**, 1272 (2011).
[23] W. Ge, H. Ohta, C. Michioka, and K. Yoshimura, J. Phys. (Conf. Seri.) **344**, 012023 (2012).
[24] R. Troć, M. Pasturel, O. Tougait, A. P. Sazonov, A. Gukasov, C. Sułkowski, and H. Noël, Phys. Rev. B **85**, 064412 (2012).
[25] S. Nakamura, S. Toyoshima, N. Kabeya, K. Katoh, T. Nojima, and A. Ochiai, JPS Conf. Proc. **3**, 014004 (2014).
[26] C. Kittel, in *Introduction to Solid State Physics*, 7th ed. (Wiley, New York, 1996), Chap. 5, p. 122.
[27] In the previous paper (Ref. [25]), we fitted the data within the range $1.8 < T < 10$ K and ontained $\Theta = -1.3$ K. However,

influence of the phase transition at $T_2 = 1.6$ K is shown in the range $1.8 < T < 2.2$ K. We then fitted the data in the range $2.2 < T < 10$ K in the present study.
[28] W. Ge, C. Michioka, H. Ohta, and K. Yoshimura, Soli. Stat. Commun. **195**, 1 (2014).
[29] J. M. Kosterlitz and D. J. Thouless, J. Phys. C **6**, 1181 (1973).
[30] J. Villain, J. Phys. C **10**, 1717 (1977).
[31] S. Teitel and C. Jayaprakash, Phys. Rev. B **27**, 598 (1983).
[32] M. Hasenbusch, A. Pelissetto, and E. Vicari, Phys. Rev. B **72**, 184502 (2005).
[33] S. Okumura, H. Yoshino, and H. Kawamura, Phys. Rev. B **83**, 094429 (2011).
[34] S. Miyashita and H. Shiba, J. Phys. Soc. Jpn. **53**, 1145 (1984).
[35] S. Lee and K.-C. Lee, Phys. Rev. B **57**, 8472 (1998).
[36] S. E. Korshunov, Phys. Rev. Lett. **88**, 167007 (2002).
[37] J.-H. Park, S. Onoda, N. Nagaosa, and J. H. Han, Phys. Rev. Lett. **101**, 167202 (2008).
[38] T. Obuchi and H. Kawamura, J. Phys. Soc. Jpn. **81**, 054003 (2012)
[39] S. E. Korshunov, Phys. Rev. B **65**, 054416 (2002).
[40] K. Kadowaki and S. B. Woods, Solid State Commun. **58**, 507 (1986).
[41] N. Tsujii, H. Kontani, and K. Yoshimura, Phys. Rev. Lett. **94**, 057201 (2005).
[42] T. Furuno, N. Sato, S. Kunii, T. Kasuya, and W. Sasaki, J. Phys. Soc. Jpn. **54**, 1899 (1985).
[43] N. Sato, A. Sumiyama, S. Kunii, H. Nagano, and T. Kasuya, J. Phys. Soc. Jpn. **54**, 1923 (1985).
[44] K. Andres, J. E. Graebner, and H. R. Ott, Phys. Rev. Lett. **35**, 1779 (1975).
[45] P. Gegenwart, J. Custers, C. Geibel, K. Neumaier, T. Tayama, K. Tenya, O. Trovarelli, and F. Steglich, Phys. Rev. Lett. **89**, 056402 (2002).
[46] T. Takimoto and T. Moriya, Soli. Stat. Commun. **99**, 457 (1996).